Phys Chem Minerals (2006) 33: 145–159
DOI 10.1007/s00269-006-0061-6

ORIGINAL PAPER

N. Tomašić · A. Gajović · V. Bermanec
D. S. Su · M. Rajić Linarić · T. Ntaflos
R. Schlögl

Recrystallization mechanisms of fergusonite from metamict mineral precursors

Received: 16 September 2005 / Accepted: 9 December 2005 / Published online: 14 February 2006

Abstract The metamict state and recrystallization of fergusonite in metamict natural samples were studied by thermal methods (TGA-DTA), X-ray powder diffraction (XRD), Raman spectroscopy (RS), transmission electron microscopy (TEM), selected area electron diffraction (SAED), and electron microprobe (EPMA). Two metamict mineral samples of fergusonite were investigated in order to identify the original premetamict crystal structure and to identify recrystallization mechanisms. The TEM data and RS provided evidence on the partial preservation of the original structure in the investigated minerals, which are X-ray amorphous. It was shown that fergusonite could recrystallize from a metamict mineral with original fergusonite structure or from metamictized pyrochlore, which was altered before or after metamictization. Two recrystallization mechanisms were recognized: (a) epitaxial growth occurring at the boundary between preserved premetamict structure fragments and completely metamictized areas, and (b) nucleation-crystal growth mechanism occurring in completely amorphous areas of the minerals, and resulting in recrystallization of the original mineral as well as in the crystallization of a new mineral with a modified chemical composition as compared to the initial matrix.

Keywords Fergusonite · Metamict state · Recrystallization mechanisms · Raman spectroscopy · TEM

N. Tomašić (✉) · V. Bermanec
Faculty of Science, Institute of Mineralogy and Petrography, University of Zagreb, Horvatovac bb, 10000, Zagreb, Croatia
E-mail: ntomasic@jagor.srce.hr
Tel.: +385-1-4605909
Fax: +385-1-4605998

A. Gajović
Rudjer Bošković Institute, POB 180, 1002, Zagreb, Croatia

D. S. Su · R. Schlögl
Fritz Haber Institut der Max-Planck-Geselschaft, 14159, Berlin, Germany

M. Rajić Linarić
Brodarski Institut, 10000, Zagreb, Croatia

T. Ntaflos
Department of Geological Sciences, University of Vienna, Althastr. 14, 1090, Vienna, Austria

Introduction

Fergusonite is a mineral frequently found in the metamict state, and chemically described with a general chemical formula ABO_4 (A = REE, Ca, U and Th; B = Nb, Ta and Ti). Fergusonite-like phases encompass a large number of synthetic compounds which are of interest due to their dielectric properties.

Two structures have been reported for fergusonite mineral samples. Komkov (1959) determined the scheelite-type structure for the tetragonal fergusonite from Urals with the space group $I4_1/a$, later named α-fergusonite (Gorshevskaya et al. 1961) or T phase for synthetic $YNbO_4$ analogues (Yashima et al. 1997). On heating at 1,000°C, the mineral transforms to a monoclinic phase with the $I2$ space group and distorted scheelite structure, named β-fergusonite (Gorshevskaya et al. 1961) or M phase in synthetic fergusonite (Markiv et al. 2002). Komkov (1959) suggested tetrahedral coordination for B-cations in both α- and β-fergusonite, while Weitzel and Schröcke (1980) refined the structure of synthetic β-fergusonite ($YNbO_4$), and proposed the space group $C2/c$ with 4 + 2 coordination for B-cations. Blasse (1973) investigated vibrational spectra of both $YNbO_4$ and $YTaO_4$ having β-fergusonite structure, and observed fewer bands than expected by symmetry considerations. This was explained by a slight distortion of β-fergusonite structure from sheelite structure that has higher symmetry. Additionally, another monoclinic fergusonite phase named M′ phase was determined for synthetic $YTaO_4$ (Wolten and Chase 1967) with the $P2/a$ space group. This phase is obtained for the crystals grown below the M–T transformation temperature (Wolten

1967). For fergusonite-related compounds like $YbTaO_4$, which are synthesized by heating co-precipitated hydroxides (Markiv et al. 2002), the primary amorphous state was observed up to 800°C where the material crystallizes with fluorite structure. At 1,000°C, it transforms to M′-fergusonite phase, and at 1,300°C the M′-phase predominates. As stated by the authors, the fluorite structure can be expected for this type of synthesis if the lanthanides with smaller ionic radii (lanthanides from Nd to Lu) are considered for an $LnTaO_4$ compound. M′-fergusonite phase transforms to M′-fergusonite by melt quenching.

Metamictization is a term synonymously used for amorphization, especially in minerals, a process that is related to heavy-particle irradiations (Ewing 1994). The resulting metamict state is an almost inherent property of complex REE–Nb–Ta oxides, due to the frequent substitution of U and Th for large REE cations in the crystal structure. In the α-decay series of U and Th, α-particles and α-recoil nuclei are ejected in opposite directions from decaying nuclei. On their trajectory, they transfer energy to the atoms in the crystal structure. The energy transfer occurs as two major processes: (a) ionization and electronic excitation, which predominantly occur in interaction of α-particles with electrons, and (b) elastic collisions of both α-particles and α-recoil nuclei with the atomic nuclei (Ewing 1987; Ewing et al. 2004). The α-particles with energy of 4.5–5.8 MeV can cause self-heating, electron-hole pairs responsible for bond rupture, charge defects, enhanced self-ion and defect diffusion, localized electronic excitations, and in some cases, defects from radiolysis (Weber et al. 1998). Along with ionization, α-particles can cause several hundred atomic displacements through elastic atomic collisions, which form Frenkel defects over a range of 16–22 μm. Significantly greater amount of displacements is produced by less energetic α-recoil nuclei (70–100 keV), whereby up to 2,000 displacements are highly localized in a displacement cascade (30–40 nm) (Weber et al. 1998; Gögen and Wagner 2000). Final amorphization of heavily irradiated materials can be achieved by several mechanisms: (a) point defect accumulation (homogeneous amorphization) (Gong et al. 1996), (b) interface-controlled amorphization (Motta 1997), (c) cascade overlap amorphization (Gibbons 1972), and (d) in-cascade amorphization (heterogeneous amorphization) (Weber 1993).

Radiation damage in oxide minerals and their synthetic analogues has been mainly investigated in pyrochlore, zirconolite, perovskite, and brannerite. Lumpkin and Ewing (1988) observed the features and stages of crystalline-metamict transition in natural pyrochlore samples with different degrees of metamictization, ranging from completely crystalline to completely amorphous. Upon ion irradiation, the pyrochlore structure transforms to a disordered fluorite structure prior to amorphization (Wang et al. 1999), which after further irradiation results in amorphous nano-domains (Wang et al. 2000). Later investigation of Lian et al. (2003) confirmed order–disorder transition in ion-irradiated pyrochlore suggesting primary disordering in anion array followed by cation disordering. Begg et al. (2001) found that $Gd_2(Ti_{2-x}Zr_x)O_7$ pyrochlores with ionic radii ratio of A- and B-site cations $r_a/r_b > 1.52$ become increasingly unstable with respect to amorphous state under irradiation which transforms the same pyrochlores with $r_a/r_b \leq 1.52$ to a radiation resistant defect-fluorite structure. Brannerite and brannerite-type ceramics seem to be less resistant to heavy-ion irradiation, what is generally explained by their lower structural connectivity in comparison with that of pyrochlore (Lumpkin et al. 2001; Yudintsev et al. 2001). Zirconolite and perovskite show the highest resistance to radiation damage among oxides (Sinclair and Ringwood 1981; Yudintsev et al. 2001). Additionally, radiation resistance in natural minerals seems to be higher than in their synthesized ceramic analogues amorphized in ion-beam facilities, what can be related to the thermal history of minerals and corresponding restoration of crystal structure, as shown in zirconolite (Ewing and Wang 1992). For oxide ceramics, which are considered radiation-resistant, like spinel, it was found that amorphization can be induced even at low temperatures if stable and nucleated defects exist in the crystal structure (Bordes et al. 1995). Trachenko et al. (2004) suggested that a complex material can be amorphized if "it is able to form a covalent network".

Radiation resistance of silicate and phosphate minerals with monazite and zircon structures has been also investigated. Generally, it was found that minerals with monazite structure recrystallize more readily, and are less susceptible to radiation damage in comparison with their silicate counterparts (Meldrum et al. 1997, 1998, 1999, 2000; Nasdala et al. 2001; Seydoux-Guillaume et al. 2002). Stability of orthophosphates seems to be related to the strength of P–O bonds in tetrahedral coordination, which is stronger in comparison with Si–O bond in the same coordination, for instance in zircon (Meldrum et al. 1996). This is also true for xenotime, which, although having the same structure as zircon, displays a radiation resistance equivalent to that of monazite (Karioris et al. 1982). Recrystallization of naturally metamict zircon is highly dependent on the degree of metamictization (Capitani et al. 2000): heavily metamictized samples start to recrystallize at higher temperatures leaving "pockets" of SiO_2 glass beside zircon crystallites. That is not the case with partly metamictized zircon samples, which show complete recrystallization. Rios et al. (2000) used the intensity of X-rays scattered from amorphous regions to determine the content of amorphous material in natural zircon, which was subsequently related to the received radiation dose. Annealing experiments of metamict zircon samples showed an enhanced rate of recrystallization if it is performed in hydrothermal conditions (Geisler et al. 2003a). It is suggested that water has "catalytic" properties in structural recovery of metamict zircon, whereby it difuses into amorphous regions and enhances

solid-state recrystallization (Geisler et al. 2003c). Recrystallization in hydrothermal conditions was also shown to be efficient for heavily metamictized samples of allanite and gadolinite (Janeczek and Eby 1993). However, zircon shows anomalous increase of diffusion-based alteration rate in hydrothermal conditions, which is related to two critical concentrations of amorphous domains: (1) amorphous domains are interconnected into clusters in the crystal structure, and (2) strongly overlapping α-recoil events form nano-sized regions of depleted matter, which serve as fast diffusion pathways (Geisler et al. 2003b). Under high pressures (3–7 GPa) radiation-damaged zircon samples show temporary increase of diffraction maxima attributed to reorientation of crystalline domains. However, the starting profile is recovered after pressure relaxation, indicating no significant defect healing within the studied pressure range (Rios and Boffa-Ballaran 2003).

The complexity of the crystal structure, where the structure is more complex if it has more cation sites, could play a significant role in metamictization of complex silicate structures. Wang et al. (1991) investigated the amorphization of neptunite, titanite, gadolinite, zircon and olivine, showing that the critical amorphization dose is lower if the structure is more complex.

Detailed studies of ion beam induced amorphization in oxides, silicates and phosphates have been performed in order to assess critical amorphization dosages, and to study the amophization/recrystallization mechanisms. This is useful in the preparation of radiation resistant ceramics used for immobilization of actinides in nuclear waste disposal.

The aim of the present study is to investigate the features of fergusonite recrystallization from heavily metamictized mineral samples. In particular, the following problems are going to be considered: (a) the possible preservation of the fragments of the original structure in the metamict mineral, and its identification, (b) recrystallization mechanisms, (c) structure changes during recrystallization, and (d) efficiency of the original phase recrystallization regarding possible alteration during and after metamictization.

Experimental

Samples and recrystallization procedure

Two mineral samples predetermined as fergusonite were investigated in this work. The samples originate from granitic pegmatites of Bakkane-Steane in Norway (sample FER-BS) and Ytterby in Sweden (sample FER-YT). The sample FER-BS was obtained from the collection of Mineralogical-geological Museum of University in Oslo, while the sample FER-YT was from Natural History Museum in Zagreb (sample No. 2021).

Preliminary X-ray diffraction (XRD) analysis indicated that both minerals are heavily metamictized. Therefore, they were gradually recrystallized in air at 400, 500, 650, 800 and 1,000°C for 24 h in each case. Additionally, the minerals were heated at 1,300°C for 6 h. The same portion of the investigated samples was used for each annealing step.

Sample characterization

Unheated and heated sample portions were investigated by X-ray powder diffraction (XRD), thermal methods (TGA-DTA), Raman spectroscopy (RS), transmission electron microscopy (TEM), and selected area electron diffraction (SAED). The unheated samples were chemically characterized by electron probe microanalysis (EPMA).

The XRD data were obtained on Philips PW 3040/60 X'Pert PRO powder diffractometer using CuKα radiation ($\lambda = 1.54055$ Å) at 45 kV and 40 mA. The incident beam was passed through an X-ray mirror with a divergence slit of 0.5°. The diffracted beam was directed to the detector through a parallel plate collimator with an equatorial acceptance angle of 0.18°. The powdered mineral samples were mounted on a single silicon crystal disc cut in a way to avoid lattice planes, and thus causing no silicon diffraction and low background. The disc with a sample was inserted into the sample spinner programmed to a revolution time of one second. Step size was set to 0.02° with measuring time of two seconds per step.

Thermal analyses were performed in a nitrogen atmosphere. The thermal data were used for the determination of water content, but also to characterize processes occurring during recrystallization. TGA and DTA curves were recorded in the range from room temperature up to 1,300°C and a heating rate of 5°C min^{-1} on a TA Instruments SDT Model 2960.

Raman spectra were recorded using computerized DILOR Z24 triple monochromator with a Coherent INNOVA 400 argon ion laser, operating at 514.5 nm line for excitation. An Anaspec's doublepass prism premonochromator was used to reduce parasite laser plasma lines. Laser power of 100 mW was applied. To reduce the heating of the sample during recording Raman spectra, the shape of the incident laser beam was altered in line focus. Raman spectra were recorded from 70 to 1,000 cm^{-1}. To check for the luminescence, the samples heated at 1300°C were additionally recorded by 488 nm line of the same system but also by Fourier transform Raman system (FTRS) Perkin Elmer GX Spectrum with Nd:YAG laser operating at 1,064 nm and power ranging from 100 to 130 mW.

TEM, SAED and high-resolution TEM (HRTEM) were performed on Philips CM200 LaB_6 and FEG microscopes, both operated at 200 kV. SAED apertures of 40 and 200 nm and camera length of 950 mm were used. For TEM measurements the ground fergusonite samples were suspended in chloroform, treated in an ultrasonic bath, applied to the carbon-coated copper

grid, and dried in air. Determination of the interplanar spacings d from the SAED patterns and phase identification of the polycrystalline domains in the samples were performed using software Process Diffraction (Lábár 2000). HRTEM images were analyzed by Digital Micrograph software (Gatan 1999).

Chemical analyses of the samples were performed with Cameca SX100 electron microprobe. The electron beam was 1 μm in diameter, excited by 20 kV with a beam current of 20 nA. For quantification the following standards were used: Nb-metal, Ta_2O_5, rutile, Fe-metal, wollastonite, UO_2, $Y_3Al_5O_{12}$ and a set of four REE alumosilicate glasses (Drake and Weill 1972). PAP correction (Pouchou and Pichoir 1991) was applied to measured data.

Results

Chemical composition

Chemical composition and structural formulae calculated on the basis of four oxygens are presented in Table 1. In case of fergusonite from Bakkane-Steane (FER-BS), the presented weight percentages of the oxides are mean values of five EMPA point analyses with standard deviation values shown in parantheses. The composition of fergusonite from Ytterby (FER-YT) is given as ranges of oxide content for seven EMPA point analyses due to a significant elemental variation, although the total and chemical formula are calculated from mean oxide values. FER-BS is evidently fergusonite-(Y), while the chemical data for fergusonite from Ytterby (FER-YT) were not so easy to interpret due to a significant compositional variation observed among EPMA point analyses. FER-YT predominantly contains Ta instead of Nb, meanwhile A-cation content shows elemental variation especially in Ca, Fe and Y.

Table 1 Microprobe analyses and structural formulae calculated on four oxygen basis for FER-BS and FER-YT

	Fergusonite-(Y) Bakkane-Steane (FER-BS)	Fergusonite-(Y) Ytterby (FER-YT)
Chemical composition in wt% (σ)		
CaO	1.91 (0.47)	5.58–11.04
FeO	0.11 (0.09)	0.58–2.19
UO_2	4.9 (0.46)	1.07–2.58
La_2O_3	< 0.05	
Ce_2O_3	0.61 (0.06)	0.05–0.12
Nd_2O_3	1.35 (0.08)	< 0.05
Sm_2O_3	1.64 (0.13)	0.07–0.18
Eu_2O_3	< 0.05	< 0.05
Gd_2O_3	1.42 (0.04)	0.21–0.37
Tb_2O_3	0.43 (0.25)	0.05–0.16
Dy_2O_3	2.31 (0.02)	0.62–1.19
Er_2O_3	0.37 (0.12)	0.42–1.44
Tm_2O_3	0.30 (0.11)	0.91–1.45
Yb_2O_3	0.27 (0.08)	1.67–5.28
Y_2O_3	32.1 (0.63)	8.38–22.30
TiO_2	1.20 (0.13)	0.61–1.12
Nb_2O_5	44.1 (1.01)	4.52–10.32
Ta_2O_5	6.5 (0.32)	43.00–57-24
H_2O	1.96	8.12
Total	101.58	98.00
Structural formula (four oxygen basis)		
Ca	0.091	0.481
Fe	0.004	0.071
U	0.049	0.024
La	< 0.001	
Ce	0.010	0.001
Nd	0.021	0.001
Sm	0.025	0.002
Eu	< 0.001	< 0.001
Gd	0.021	0.005
Tb	0.006	0.002
Dy	0.033	0.017
Er	0.005	0.016
Tm	0.004	0.023
Yb	0.004	0.056
Y	0.756	0.483
A cations	1.029	1.183
Ti	0.040	0.037
Nb	0.882	0.172
Ta	0.078	0.794
B cations	1.000	1.003

Thermal data

Thermal data for both samples indicated the start of recrystallization at temperatures higher than 400°C (Figs. 1, 2). DTA and TGA curves show that dehydration precedes recrystallization. This is in a correspondence with the recrystallization of the mineral in the case of metamictization accompanied with hydration. Therefore, the variability of the DTA curve could be ascribed to a competition between these two processes opposite in enthalpy character. The water content is significantly different between the two samples, as inferred from the weight loss. Although FER-BS showed significantly lower loss of weight in comparison with FER-YT, it was losing mass over the whole temperature range.

The TGA curve for FER-BS shows two major steps of weight loss (1.25 and 0.71%), which are always followed by stepwise recrystallization, and at least five exothermic maxima could be observed up to 800°C on DTA curve (200.00, 522.14, 582.14, 687.27 and 767.27°C). The weight loss of 1.25% is apparently related to the loss of adsorbed and absorbed (metamict) water in the mineral, which is accomplished at approximately 800°C. As shown later by XRD measurements (Fig. 3), this temperature range is characterized by the recrystallization of α-fegusonite. Accordingly, the five exothermic maxima should be attributed to this recrystallization, and indicate temperature points in which recrystallization dominates over dehydration. The remaining two exothermal maxima occurring at temperatures above 800°C (1,080°C and the incomplete one at the end of the heating range) can be related to the phase transition from tetragonal α- to monoclinic β-fergusonite and a

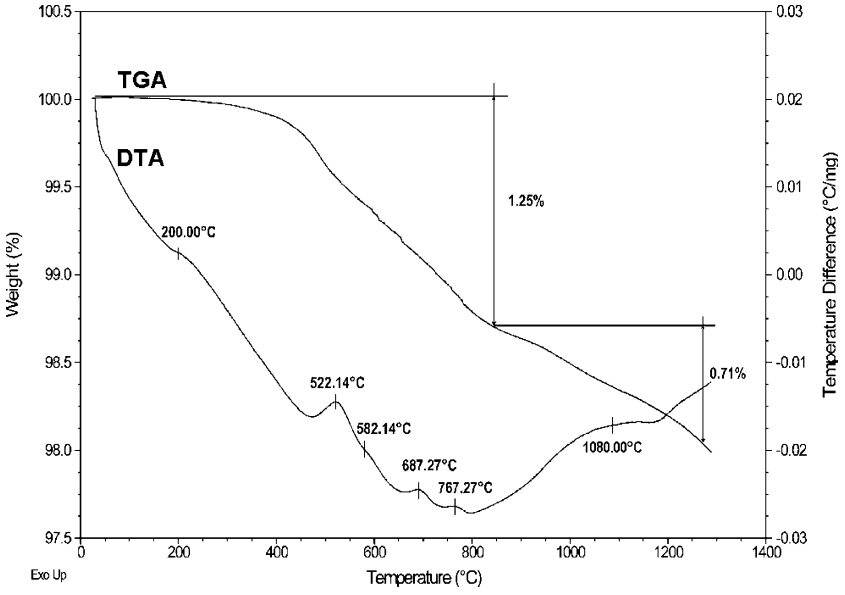

Fig. 1 TGA and DTA diagrams for FER-BS

corresponding increase in crystallinity of β-fergusonite, as inferred from XRD patterns (Fig. 3).

For FER-YT the dehydration ends in the range 600–800°C, enabling faster recrystallization at higher temperatures, resulting in three exothermic maxima above 700°C (756.04, 975, 1159.52°C); (Fig. 2). The maximum at 756.04°C may be assigned to the faster recrystallization of pyrochlore phase after the majority of metamict water is expelled. The exothermic maximum at 975°C should be related to the crystallization of β-fergusonite, what corresponds to the diffraction pattern at 1,000°C (Fig. 4). The last exothermic maximum (1,159.52°C) is most likely a consequence of further increase in crystallinity and grain coarsening of both pyrochlore phase and β-fergusonite. Significant decrease in mass may be attributed both to the loss of molecular water but also of OH^- group which is structurally bounded in the pyrochlore structure present in this sample (as shown later).

The TGA-DTA data for both samples indicate an enhanced rate of recrystallization after each step of dehydration. The thermogravimetric curves show more or less continuous loss of water or OH^- group with temperature increase. This is represented by a negative slope of DTA curve up to approximately 700–800°C, indicating a dominant influence of an endothermic process, apparently dehydration. A series of exothermic maxima superposed over this endothermic "background" should be related to the temperature points of more intensive recrystallization favored by achieved temperature and content of expelled water. The loss of mass even at high temperatures, for instance 0.71% in the case of FER-BS (Fig. 1), suggests that metamict water could be trapped in the mineral interior, indicating

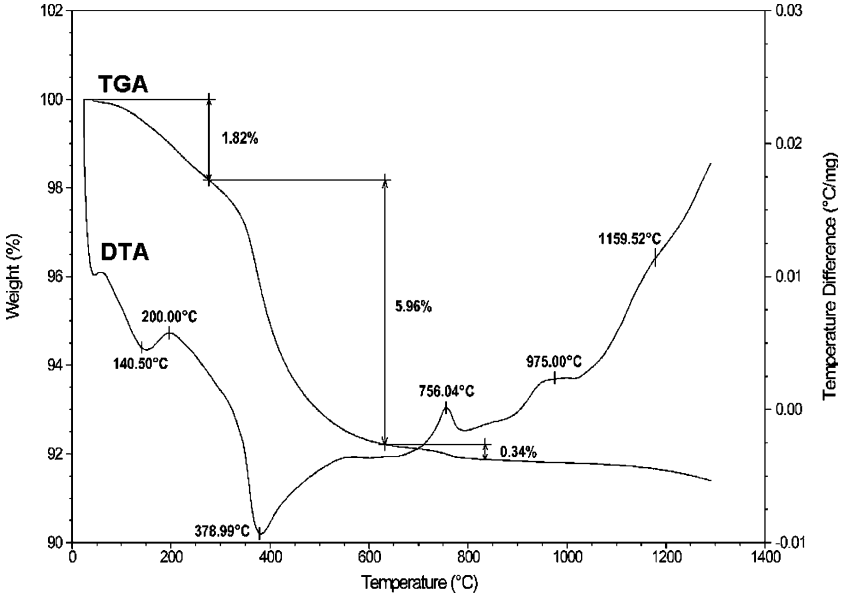

Fig. 2 TGA and DTA diagrams for FER-YT

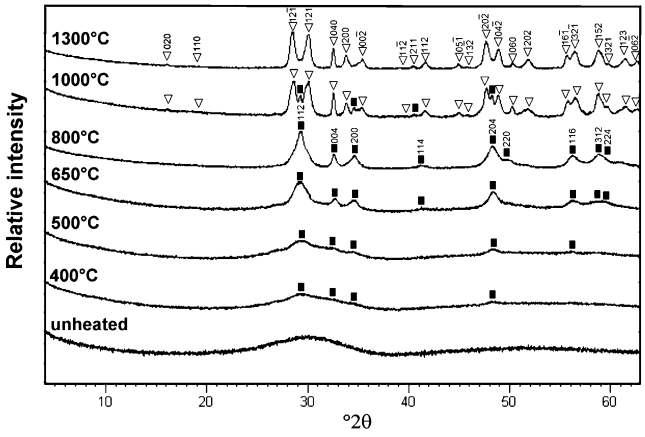

Fig. 3 XRD patterns for unheated and heated FER-BS (*filled boxes* α-fergusonite, *inverted triangle* β-fergusonite)

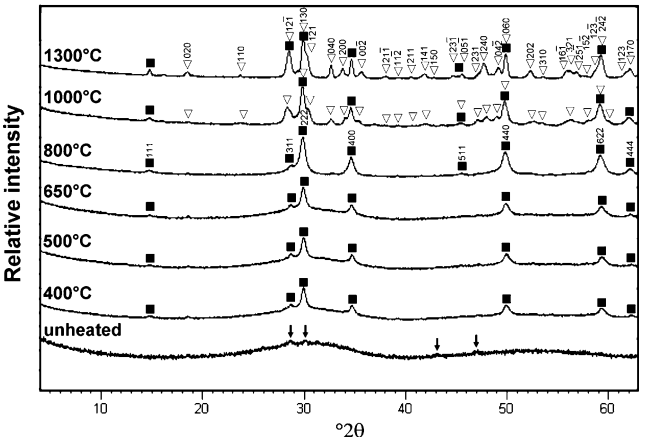

Fig. 4 XRD patterns for unheated and heated FER-YT (*filled boxes* pyrochlore, *inverted triangle* β-fergusonite

its significant penetration into the porous metamict structure. On the other hand, the weight loss at such high temperatures may indicate the escape of other volatiles, whereby oxygen could be a reasonable candidate due to the thermal expansion of the crystal lattice or thermal reduction of certain elements at high temperature.

X-ray powder diffraction

X-ray powder diffraction patterns indicated different recrystallization paths for the investigated samples. FER-BS was completely X-ray amorphous (Fig. 3). Heating treatment induced recrystallization starting at 400°C. At the beginning the mineral recrystallized tetragonally with the space group $I4_1/a$ (α-fergusonite) as suggested in previous investigations (Berman 1955; Komkov 1959). XRD patterns (Fig. 3) showed that the degree of crystallinity increased as the heating temperature was increased. The recrystallization continued up to 1,000°C, when the transition to the monoclinic (space group *I2*) β-fergusonite phase began. However, the presence of the most intense diffraction lines of the α-fergusonite indicated incomplete phase transition. The prolonged heating up to 1,300°C completely eliminated α-fergusonite and the phase transition to β-fergusonite was completed. This phase transition was in accordance with previous observations for the natural fergusonite samples (Komkov 1959; Gorshevskaya et al. 1961).

The diffraction data for FER-YT indicated the mineral not to be completely metamict (Fig. 4). A few diffraction lines of very low intensity were observed for the unheated sample. The lines coincided with those of pyrochlore structure (space group $Fd\bar{3}m$). The recrystallization of pyrochlore structure was continuously monitored with temperature increase starting at 400°C. The pyrochlore phase was stable up to 1,300°C. However, another phase resembling β-fergusonite started to crystallize at 1,000°C. By heating the sample to 1,300°C the presence of β-fergusonite was clearly observed. The identification of β-fergusonite was hindered by the overlap of its major diffraction maxima (3.12 and 2.95 Å) with those of pyrochlore. Therefore, a careful characterization of low intensity lines was made in order to warrant a reliable mineral identification.

The observed differences in recrystallization for the two samples may be related to the previously shown thermal data: FER-YT is more reactive due to the higher amount of H_2O/OH^-, while FER-BS is more "polymerized" and hence less reactive. As shown by Geisler et al. (2003a), water can enhance solid-state recrystallization after diffusing into amorphous domains of metamict zircon.

The recrystallization of metamict minerals also changes unit cell parameters of recrystallizing phases. For both investigated samples phases recrystallizing first i.e. α-fergusonite in FER-BS and pyrochlore phase in FER-YT, show an increase of unit cell volume up to 1,000°C (Table 2). When compared to TGA-DTA data (Figs. 1, 2), this can be related to the prolonged and stepwise dehydration occurring during recrystallization. The stepwise dehydration can cause a discontinuity in the recrystallization process, since the water can temporarily distort the crystal lattice due to the random paths of its escape from the metamict mineral. The recrystallization of zircon showed that water can assist faster structure recovery (Geisler et al. 2003a) but could also be a barrier to recrystallization (Geisler et al. 2003c). Above 1,000°C, the unit cell parameters and consequently the volume of unit cell for β-fergusonite decrease, indicating progressive increase in crystallinity as the temperature rises.

However, there is a difference in unit cell volume for the final β-fergusonite recrystallizing from the two samples, where the volume of FER-BS is much closer to the reference value ($V = 292.52$ Å^3, PDF 23–1486, ICDD 2004) (Table 2). This difference can be explained by the differences in chemical composition between two samples, especially if the dominant B-site cations are

Table 2 Unit cell parameters of the investigated fergusonite samples

Mineral	t (°C)	Space group [a]	*a* (Å)	*b* (Å)	*c* (Å)	*β* (°)	Volume (Å^3)
Fergusonite-(Y) Bakkane-Steane (FER-BS)	400	$I4_1/a$	5.10(2)		10.92(4)		284(2)
	500	$I4_1/a$	5.16(2)		11.00(4)		293(2)
	650	$I4_1/a$	5.196(4)		10.96(1)		296.8(5)
	800	$I4_1/a$	5.174(1)		10.965(2)		293.5(1)
	1,000	$I2$	5.297(3)	10.956(8)	5.077(4)	94.27(6)	293.9(2)
	1,300	$I2$	5.299(2)	10.970(4)	5.062(3)	94.34(5)	293.4(2)
Fergusonite-(Y) Ytterby (FER-YT)	400	$Fd\bar{3}m$	10.322(4)				1100(1)
	500	$Fd\bar{3}m$	10.326(2)				1100.9(6)
	650	$Fd\bar{3}m$	10.339(3)				1105.2(9)
	800	$Fd\bar{3}m$	10.342(1)				1106.3(3)
	1,000	$Fd\bar{3}m$	10.336(6)				1104(2)
		$I2$	5.248(5)	10.890(6)	5.067(5)	94.96(8)	288.5(3)
	1,300	$Fd\bar{3}m$	10.326(2)				1100.9(8)
		$I2$	5.277(5)	10.905(7)	5.021(4)	94.64(6)	288.0(2)

[a] $I4_1/a$ α-fergusonite, $I2$ β-fergusonite, $Fd\bar{3}m$ pyrochlore

considered (Table 1). Keller (1962) calculated unit cell parameters for all the niobates and tantalates with β-fergusonite structure having REE as A-site cations. The data presented there generally showed that the *a* parameter and angle *β* had higher values while parameters *b* and *c* had lower values for tantalates in comparison with those of their niobate counterparts. However, pure $YNbO_4$ had all parameters higher, with exception of angle *β*, when compared to pure $YTaO_4$. If we calculate the unit cell volume using unit cell parameters given by Keller (1962), we obtain V = 292.45 Å^3 for pure $YNbO_4$ and V = 287.2 Å^3 for pure $YTaO_4$. These values are quite close for those of niobium-dominant FER-BS and tantalum-dominant FER-YT respectively (Table 2).

Raman spectra

Raman spectra for both investigated samples indicated gradual recrystallization with an increase of heating temperature (Figs. 5, 6). Similar behavior is observed for the metamict minerals of the aeschynite and euxenite group (Tomašić et al. 2004)

Although unheated FER-BS was X-ray amorphous (Fig. 3), the Raman spectrum showed broad bands at 779, 685, 697, 310, 208 and 108 cm^{-1} (Fig. 5). This can be related to the partial preservation of a premetamict structure in this sample. The observed bands can be assigned to stretching and bending modes of the $(Nb,Ta)O_4$ tetrahedron (Blasse 1973) in fergusonite with scheelite structure (α-fergusonite).

At lower heating temperatures (400 and 500°C) the bands unpredictably broadened, and the intensity decreased probably due to the disordering in the preserved structure fragments during the removal of the water, as indicated by TGA-DTA curves (Fig. 1). After heating at 650°C the broad bands regained their intensity. Once heated to 800°C the band splitting occurred as expected due to the transition to *β*-fergusonite and concomitant lowering of the symmetry. The bands were better resolved after heating at higher temperatures and the Raman spectrum obtained after heating at 1,300°C generally corresponds to the synthetic $YNbO_4$ with *β*-fergusonite structure recorded by Yashima et al. (1997) (Table 3).

Raman spectra of FER-YT from the unheated sample, and after heating at 400 and 500°C, did not show any Raman bands, thus indicating amorphous features of the material (Fig. 6). FER-YT sample heated at 650°C had a spectrum with broad bands of shapes and positions similar to the spectrum of FER-BS. After heating at 800°C Raman bands of both samples were at the same position, but their relative intensity was different. Moreover, the bands of FER-YT were broader than FER –BS bands, thus indicating lower crystallinity.

Raman spectra of both samples heated at 1,000 and 1,300 °C showed significant band splitting due to the decrease of fergusonite symmetry to *β*-fergusonite or the occurrence of *β*-fergusonite along with pyrochlore phase, but also this could be affected by the occurrence of luminescence lines. The samples heated at 1,300 °C were investigated by two Raman systems with different excitations (Ar 514.5 nm and 488 nm lines for dispersive RS, and Nd:YAG 1,064 nm line for FTRS) to check for possible luminescence lines in the spectra. The spectra of both samples recorded by 1,064 nm line contained fewer bands than the spectra recorded by 514.5 nm (Table 3). By comparing position and intensity of the bands absent in FTRS (at positions near 335, 350, 370, 560 and 700 cm^{-1}), it was found that the bands were not resolved by FTRS. Actually, the lower energy of 1,064 nm line could be too weak to induce all Raman active bands. On the other hand, the bands observed in FER-YT samples but not in FER-BS, could be the result of two phases present in FER-YT after heating at higher temperature (pyrochlore + *β*-fergusonite) (Figs. 5, 6). Possible luminescence is most easily detected by the comparison of bands position upon excitation with 488 nm (20,492.4 cm^{-1}) and 514.5 nm (19,435.1 cm^{-1}) lines. When the excitation line is changed to another wavelength the Raman

bands shift together with the excitation line, while the luminescence lines stay on the same absolute wavenumber. Therefore, luminescence lines observed in spectra obtained by 514.5 nm laser should appear in 488 nm spectra shifted for 1,057 cm^{-1} to higher wavenumber. Bearing that in mind, some very sharp and narrow bands were identified as luminescence, and thus indicated in Table 3. The occurrence of luminescence lines is related to the presence of REE in the crystal structure if compared to pure $YNbO_4$ showing no luminescence emission for the same excitation (Yashima et al. 1997). Also, the shape of the luminescence lines is characteristic for 4f orbital transitions characteristic for rare-earth elements (Nasdala et al. 2004b).

TEM and SAED

The TEM image of the unheated FER-BS sample (Fig. 7a) shows two different types of domains in the metamict mineral. The first type (Fig. 7a1) is clearly amorphous due to the metamictization, showing no structural patterns and only an amorphous halo on the SAED pattern. The second type of domains (Fig. 7a2) consists of isolated regions with the preserved premetamict structure. In these crystalline domains lattice fringes were observed in the HRTEM image (Fig. 7a3). The distances between fringes correspond to α-fergusonite structure. The SAED patterns (Fig. 7a2) also indicated α-fergusonite. The size of crystallites was around 10 nm and the relative fraction of crystalline areas in metamict matrix was too low to be observed by X-rays.

On heating FER-BS, the mineral recrystallizes, as shown by Fig. 7b–d. The combined analysis of HRTEM and SAED images clearly indicated the presence of two types of crystalline areas: (1) larger crystalline areas showing same orientation of lattice fringes through the whole unique grain (Fig. 7b1, d), which was sometimes idiomorphic; (2) crystalline areas containing a large number of small crystallites with random orientation (Fig. 7b2, c1) and with characteristic rings in diffraction patterns.

As in the case of FER-BS, the unheated FER-YT also contains preserved crystalline areas in a generally amorphous matrix (Fig. 8a1–a4). The crystalline domains were identified as relics of a pyrochlore phase (Fig. 8a3, a4). In FER-YT heated at 1,300°C β-fergusonite was identified by HRTEM images (Fig. 8b2). Coexistence of the pyrochlore and β-fergusonite phase in this sample was confirmed by SAED data (Fig. 8b1).

Discussion

Preservation of premetamict structure fragments

Although having characteristic XRD patterns of metamict or almost completely metamictized minerals i.e. X-ray amorphous pattern, HRTEM and SAED images demonstrated partial preservation of original premetamict crystal structure in the investigated fergusonite samples. For FER-BS (Fig. 7a3) crystalline islands of primary structure are surrounded by amorphous mineral matrix. The crystalline domains show lattice fringes with *d*-values ranging between 3.06 and 3.07 Å (Fig. 7a3) corresponding to the (1 1 2) lattice plane of α-fergusonite, which is also identified by the corresponding SAED pattern (Fig. 7a2). The observed *d*-value for (1 1 2) plane in Fig. 7a3 was higher than the reported value with $d_{112} = 3.03$ Å (PDF 88–1726, ICDD 2004), indicating a distortion of crystal lattice even in the domains with preserved structure patterns, but can also reflect variations in chemical composition.

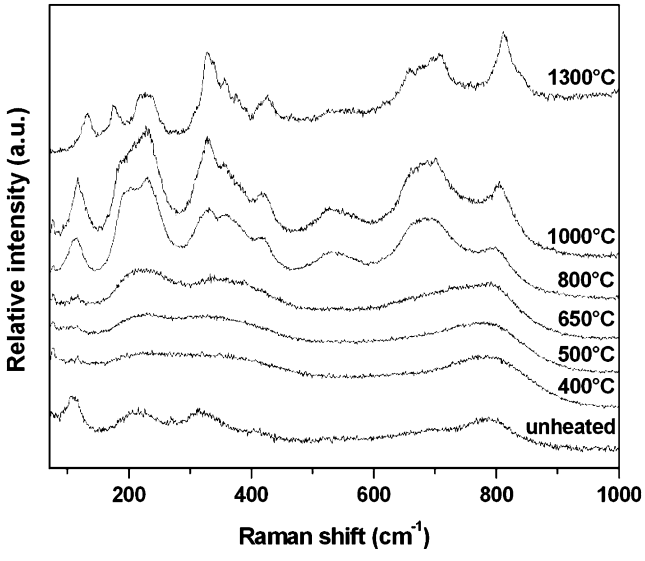

Fig. 6 Raman spectra of unheated and heated FER-YT

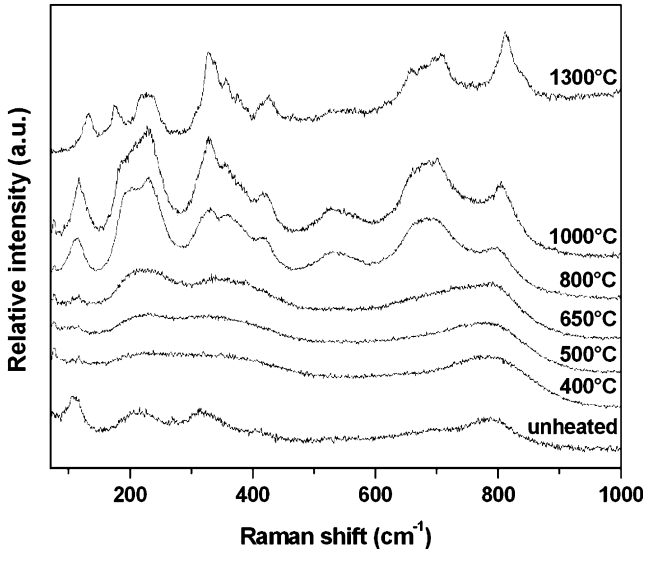

Fig. 5 Raman spectra of unheated and heated FER-BS

Table 3 Raman bands observed for FER-BS and FER-YT heated at 1,300°C

Fergusonite-(Y) Bakkane-Steane (FER-BS)			**Fergusonite-(Y) Ytterby (FER-YT)**			**$YNbO_4$ (Yashima et al. 1997)**[c]	***$Y_2Ti_2O_7$* (Glerup et al. 2001)**[d]	**Assignment (Blasse 1973)**[e]		
488 nm	*514.5 nm*	*1064 nm*	*488 nm*	*514.5 nm*	*1064 nm*	*488/514.5 nm*	*1064 nm*	*$YNbO_4$*	*$YTaO_4$*	
102[a]			103[a]	105						
124	129					131			120	external vibrations
						141				
						161				
	174[b]			164[b]		166		170		
204			196	207[b]	207					
217	218	212	218	218		213	221	225	215	
						233		245		
		276	295	296						
							309			
325	326	330	325	324	324	324	333		320	ν
	335		330	331	332	336		340		
	356[b]			350[b]				350	345	
	374[b]			370[b]		381		385	375	
418	412[b]			408[b]						ν
430	426	424		425		420				
		442			444	439	448	435		
	462	462			466	465		455	450	
								480	480	
			510	521[b]	510					
	523[b]				526		522			ν
	559[b]			559[b]				560		
							609			
658	658	657	665	657	649	658		650	655	
683	673	681		688	682	675		675	670	
	692[b]					698		695	705	
	707[b]			714[b]			720	715	720	
					733					
					747					ν
					764					
807	810	813	816	816	821	811				
	831[b]	831						832		
					843					
			891	878	893					
		917	911	924[b]	924					

ν_1 symmetric stretching, ν_2 symmetric bending, ν_3 asymmetric stretching, ν_4 asymmetric bending
[a] plasma lines,
[b] luminescence lines,
[c] *β*-fergusonite,
[d] pyrochlore structure,
[e] *β*-fergusonite, tetrahedral B-cation coordination assumed

Distortion of the lattice may be related to the defect accumulation resulting in swelling and consequent increase of the *d*-value for the (1 1 2) lattice plane. The chemical composition of the reference is simply expressed as $(Y_{0.85}Yb_{0.15})NbO_4$ (PDF 88–1726, ICDD 2004), what is, together with unit cell parameters, identical to the data published by Komkov (1959). Taking into account only this simple composition and comparing it with the chemical composition of FER-BS (Table 1), the observed *d*-value for the (112) plane is reasonably higher due to the incorporation of Ca and REE with larger ionic radii (Shannon 1976). The distortion of lattice due to a strain field and the presence of amorphous domains in many cases could be evolved from the broadening and asymmetry of diffraction maxima in the XRD pattern but also from the mottled diffraction contrast of electron diffraction images. The study of pyrochlore showed that broadening of XRD

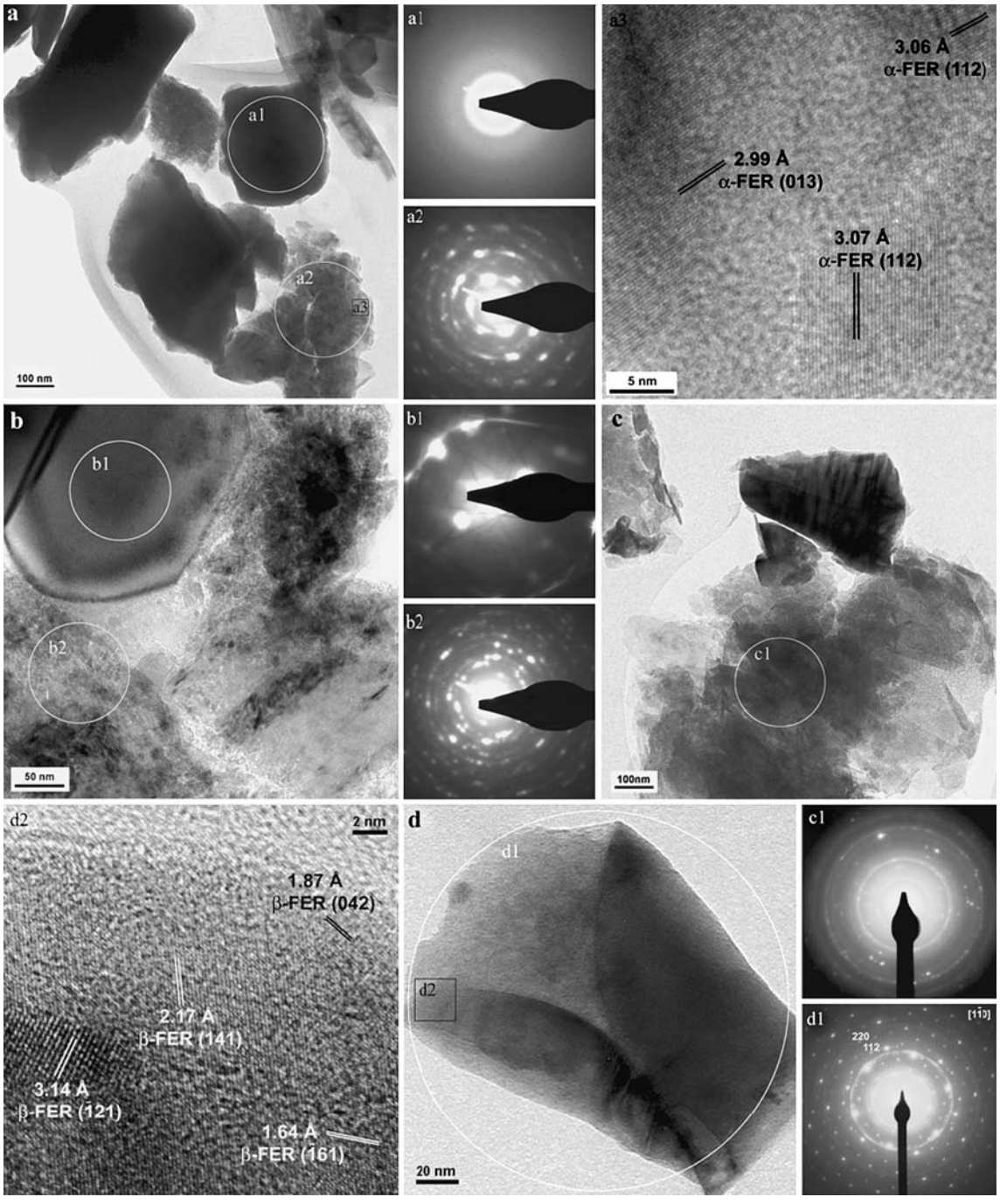

Fig. 7 TEM micrographs of FER-BS: **a** unheated sample, **b** sample heated at 1,000°C, **c** sample heated at 1300°C (small crystallites), **d** sample heated at 1,300°C (large crystallites)

lines in the first half of crystalline-to-metamict transition is mainly influenced by strain, and after that the broadening is mainly caused by a decrease in crystallite size (Lumpkin and Ewing 1988). In the case of monazite (Seydoux-Guillaume et al. 2002) the observed asymmetry of diffraction peaks was explained by co-existence of undamaged and by radiation distorted monazite lattices in the sample. In the present work the assessment of the strain and contribution of amorphous domains in the X-ray pattern could not be determined, since no diffraction maxima were recorded for thermally untreated FER-BS. The SAED pattern, however, shows diffused diffraction spots in the characteristic diffraction rings (Fig. 7a2). Diffused diffraction spots and mottled diffraction contrast can be attributed to the distortion of the preserved crystal lattice fragments and contribution of surrounding aperiodic domains to the diffraction pattern as it has been already shown in zircon (Murakami et al. 1991).

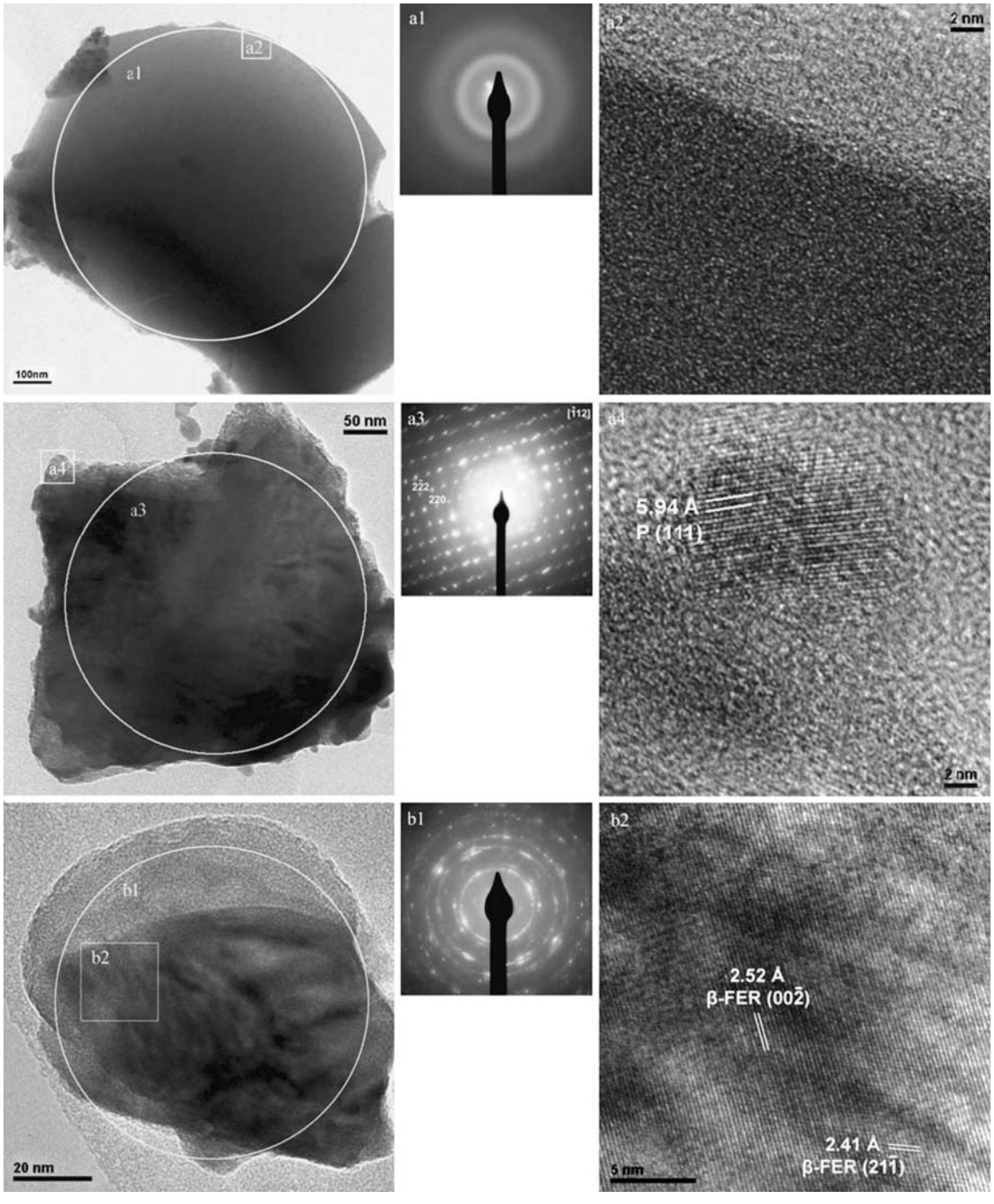

Fig. 8 TEM micrographs of FER-YT: **a** unheated sample, **b** sample heated at 1,300°C

The identification of crystalline domains in heavily metamictized FER-BS provides valuable information on the original fergusonite structure. The original structure could be also inferred from the recrystallization sequence as heating temperature rises, where α-fergusonite recrystallizes at lowest heating temperatures. Additionally, the Raman spectrum of unheated FER-BS shows a partial preservation of the structure by appearance of broad vibration bands. These bands at 779, 697, 685, 310, 208 and 108 cm^{-1} indicate the presence of short-range order in the generally metamict or X-ray amorphous mineral, and can be attributed to normal vibration stretching and bending modes in BO_4 tetrahedra in the structure of α-fergusonite (Blasse 1973).

X-ray diffraction data of the sample from Ytterby (FER-YT) show a few weak diffraction lines indicating a lower degree of metamictization (Fig. 4). The preserved

structure in the unheated sample was directly observed and identified by SAED and HRTEM (Fig. 8a3, a4). The preserved domains have pyrochlore structure. The unheated mineral contains even larger crystalline grains which, according to the SAED pattern (Fig. 8a3) have single crystal properties. Diffuse diffractions spots indicate distortion of the crystal lattice.

The present work shows that the relics of premetamict structure in naturally metamict fergusonite can be directly revealed employing HRTEM and SAED without annealing experiments. Similar has also been shown for heavily damaged zircon samples by employing TEM techniques (Weber et al. 1994; Capitani et al. 2000) and also XRD (Rios and Boffa-Ballaran 2003).

Recrystallization mechanisms

For FER-BS two recrystallization mechanisms could be identified. In the first one, as suggested by Wang et al. (2000), the presence of the preserved structural fragments gives rise to the epitaxial recrystallization on the boundary between amorphous and crystalline domains. Such a recrystallization resulted in a formation of larger crystalline areas (0.1–0.3 μm) with long-range ordering, sometimes yielding idiomorphic crystals (Fig. 7b). SAED patterns of these areas (Fig. 7b1) are characterized by the occurrence of Kikuchi lines, indicating inelastic scattering of electrons passing the thick crystallite. A large crystalline area was even more evident at higher temperatures. The corresponding SAED pattern along $[1\bar{1}0]$ axis of a grain shows long range ordering (Fig. 7d1).

The second mechanism, nucleation-crystal growth recrystallization, was identified in the largely amorphous areas of FER-BS resulting in polycrystalline domains and characteristic SAED patterns (Fig. 7b2, c1). The observed recrystallization mechanisms are analogous to those found in artificially amorphized uranium–niobium titanates (Lian et al. 2001).

In FER-YT relics of the preserved fergusonite structure were not observed. Therefore, the fergusonite structure probably appears only as a result of heating experiments. This means that there were two possible recrystallization evolutions: (a) fergusonite was present prior to metamictization, and was completely metamictized, and recrystallized after annealing experiments, and (b) pyrochlore was only original phase present in the mineral, and fergusonite crystallized within the completely amorphous areas. The former recrystallization evolution would indicate unpreferable crystallization of α-fergusonite at lower temperatures in the completely amorphous domains of the sample, so that only the recrystallization of *β*-fergusonite as a high-temperature phase was possible. The latter recrystallization evolution would presume original pyrochlore composition that was substantially altered before or after metamictization, but also a possible influence of recrystallization conditions. The alteration of the original stoichiometry was enhanced by absorbed water during and after metamictization giving opportunity to the new phases to crystallize. This alteration of the original pyrochlore structure is in correspondence with previous studies on the alteration of pyrochlore group minerals (Lumpkin and Ewing 1992, 1995, 1996).

While the crystallization of FER-BS showed only recrystallization of fergusonite-(Y) with a phase transition between tetragonal and monoclinic structure, the recrystallization of the FER-YT resulted in the co-crystallization of a pyrochlore phase and *β*-fergusonite at higher temperatures. The occurrence of *β*-fergusonite does not coincide with the observed fragments of the original pyrochlore structure in the metamict mineral, and can therefore be related to the second recrystallization mechanism (nucleation-crystal growth) in the completely metamict domains. These domains are more susceptible to change of the original stoichiometry through alteration processes. Alteration could be inferred from the significant variation in chemical composition indicated by EMPA analyses (Table 1).

Recrystallization and vibration spectra

Up to now, there have been few applications of Raman spectroscopy in the investigation of metamict minerals, whereby the majority of samples studied were related to metamict zircon and monazite (Nasdala et al. 1995; Zhang et al. 2000a, 2000b; Seydoux-Guillaume et al. 2002). Generally, Raman spectra show that metamictization causes broadening of the vibration bands, decrease in their intensity, and lowering of the frequency of stretching modes (Nasdala et al. 1995). In the present work, Raman spectra for both recrystallized samples show predictable opposite behavior as the heating temperature rises: intensifying of vibration bands and decrease of their width (Figs. 5, 6). The observed differences in spectral evolution of the investigated samples are probably a consequence of chemical variability and structural features, which are even more pronounced due to the occurrence of two phases in the sample from Ytterby at the highest annealing temperatures.

Although a mineral is X-ray amorphous, the presence of relics of former crystal structures, detectable using RS, HRTEM and SAED, is possible. In the case of FER-BS, the unheated mineral yields a few broad Raman bands. These bands indicate the preservation of short-range order along one stacking direction of the same type of M–O polyhedra in the premetamict fergusonite structure. This can be related to the observations for heavily metamictized zircon samples, for which Raman bands are still recorded due to the stability of SiO_4 tetrahedra (Nasdala et al. 1995). On the other hand, although XRD data and TEM images of unheated FER-YT indicated original structure fragments in the amorphous matrix, it is not expected that no vibration

bands in Raman spectrum would be observed, especially when compared to FER-BS. Actually, vibration bands for FER-YT are first observed not below 650–800°C. If the relation to TGA-DTA data is taken into consideration (Fig. 2), it can be noted that dehydration ends at 800°C. Also, the XRD pattern (Fig. 4) shows that at 800°C the pyrochlore phase has the highest degree of crystallinity before occurrence of β-fergusonite, and after 800°C the unit cell volume starts to decrease. Therefore, poor crystallinity of the pyrochlore phase and high water content are most likely responsible for the absence of Raman bands in the unheated FER-YT.

The occurrence of luminescence lines at higher temperatures in both samples provides additional evidence of crystal structure recovery by annealing. Pure $YNbO_4$ with β-fergusonite structure does not show luminescence lines for both 488 and 514.5 nm Ar laser excitations (Yashima et al. 1997). The studies of cubic Y_2O_3 doped with different REE showed significant luminescence properties in otherwise non-luminescent pure Y_2O_3, what is attributed to the strong crystal field splitting of 4f orbitals in REE (Laversene et al. 2001). The occurrence and increase of luminescence lines, observable in the temperature range from 1,000 to 1,300°C (Figs. 5, 6 Table 3), obviously clearly imply the formation of favorable crystal field splitting conditions for REE cations on A-site in β-fergusonite structure. This behavior is similar to the one obtained by cathodoluminescence (Nasdala et al. 2002) and laser-induced photoluminescence (Nasdala et al. 2004a) in recrystallization of metamict zircon. The recrystallization of metamict zircon induces the recovery of cathodoluminescence spectra, since the results suggest that cathodoluminescence is generally suppressed in radiation-damaged structures. The origin of cathodoluminescence seems to be related to point defects or REE^{3+} 4f electronic transitions. A possible explanation for the absence of cathodoluminescence in an unheated metamict mineral, and hence luminescence in Raman spectra, are strong disturbances of site symmetries for REE^{3+}, electronic defects in their vicinity or ionization effects due to self-irradiation. The change of luminescence properties can also be a useful tool for tracking the features of metamictization/recrystallization in Nb–Ta–REE complex oxides like fergusonite.

Conclusions

The combined study of heavily metamictized fergusonite samples using chemical characterization, thermal methods, XRD, RS, HRTEM and SAED, yielded the following conclusions:

(a) The original crystal structure of the metamict mineral can be identified in the metamict mineral using TEM techniques. SAED patterns and HRTEM images usually give sufficient information to identify the original premetamict phase. In this way, recrystallization induced by annealing experiments in order to identify metamict mineral phases is avoided, thus preventing uncertainties due to the possible oxidation, phase transition and occurrence of additional phases.
Two investigated samples assumed to be fergusonite yielded two different directly observed structures. α-fergusonite (s.g. $I4_1/a$) was identified as a premetamict structure of the sample named FER-BS, while the sample FER-YT had the original pyrochlore structure (s.g. $Fd\bar{3}m$).

(b) Two recrystallization mechanisms were observed in the investigated samples:
   - Preserved structural fragments give rise to epitaxial recrystallization on the boundary between amorphous and crystalline domains. These relics are seeds for reconstruction of the original crystal structure, and crystal growth on them results in idiomorphic grains recognized during HRTEM observations.
   - Nucleation-crystal growth recrystallization in completely metamictized domains. Completely amorphized/metamictized minerals can be easily altered, and their recrystallization can result in a completely different crystal structure, compared to the original one.

(c) FER-BS recrystallizes initially as α-fergusonite, but in the temperature range between 800 and 1,000°C undergoes the transformation from α-fergusonite to β-fergusonite. On the other hand, FER-YT recrystallizes with pyrochlore structure being present throughout the full investigated temperature range. β-fergusonite co-crystallizes at higher temperatures.

(d) Alteration before or after metamictization can change original mineral stoichiometry. Therefore, the FER-YT sample with premetamict pyrochlore structure partially recrystallized to β-fergusonite due to the alteration of original pyrochlore composition. However, the influence of the different conditions during mineral formation and annealing experiments should not be neglected.

Although not a novel technique used in mineralogy, the present study showed that transmission electron microscopy is a method of choice for investigations of metamict minerals. This is especially true for the identification of premetamict crystal structures in a metamict mineral. Many problems occurring during common identification of metamict minerals upon recrystallization, like influence of annealing conditions, oxidation, phase transitions, and occurrence of additional phases, are largely avoided by the application of TEM techniques in the investigation of untreated metamict minerals.

Acknowledgements The authors are grateful to Gunnar Raade from Geological and Mineralogical Museum in Oslo, and Vladimir Zebec from Croatian Natural History Museum for providing the mineral samples. We thank dr. Ozren Gamulin from School of

Medicine, University of Zagreb, for FT Raman measurements. The constructive comments and helpful suggestions of S. Rios and S. V. Yudintsev are gratefully acknowledged. The investigation was supported by the Ministry of Science, Education and Sport of Republic of Croatia through the grants No. 0119420 and 0098022. EMPA analyses were supported by Austrian–Croatian bilateral project. The work at TEM facility in Berlin was financially supported by the Max Planck Society.

References

Begg BD, Hess NJ, McCready DE, Thevuthasan S, Weber WJ (2001) Heavy-ion irradiation effects in $Gd_2(Ti_{2-x}Zr_x)O_7$ pyrochlores. J Nucl Mater 289:188–193

Berman J (1955) Identification of metamict minerals by X-ray diffraction. Am Mineral 40:805–827

Blasse G (1973) Vibrational spectra of yttrium niobate and tantalate. J Solid State Chem 7:169–171

Bordes N, Wang LM, Ewing RC, Sickafus KE (1995) Ion-beam induced disordering and onset of amorphization in spinel by defect accumulation. J Mater Res 10:981–985

Capitani GC, Leroux H, Doukhan JC, Rios S, Zhang M, Salje EKH (2000) A TEM investigation of natural metamict zircons: structure recovery of amorphous domains. Phys Chem Miner 27:545–556

Gatan (1999) Digital Micrograph 3.6.5. Gatan Inc., Pleasanton, CA, USA

Drake MJ, Weill DF (1972) New rare earth element standards for electron microprobe analysis. Chem Geol 10:179–181

Ewing RC (1987) The structure of metamict state. In: Konta J (eds) 2nd international conference on Natural Glasses, Prague. Charles University, Praha, pp 41–48

Ewing RC (1994) The metamict state: 1993—the centennial. Nucl Instrum Methods B 91:22–29

Ewing RC, Wang LM (1992) Amorphization of zirconolite: alpha-decay event damage versus krypton ion irradiation. Nucl Instrum Methods B 65:319–323

Ewing RC, Weber WJ, Lian J (2004) Nuclear waste disposal—pyrochlore ($A_2B_2O_7$) Nuclear waste form for the immobilization of plutonium and ''minor'' actinides. J Appl Phys 95:5949–5971

Geisler T, Pidgeon RT, Kurtz R, Van Bronswijk W, Schleicher H (2003a) Experimental hydrothermal alteration of partially metamict zircon. Am Mineral 88:1496–1513

Geisler T, Trachenko K, Rios S, Dove MT, Salje EKH (2003b) Impact of self-irradiation damage on the aqueous durability of zircon ($ZrSiO_4$): implications for its suitability as a nuclear waste form. J Phys Condens Matter 15:L597-L605

Geisler T, Zhang M, Salje EKH (2003c) Recrystallization of almost fully amorphous zircon under hydrothermal conditions: An infrared spectroscopic study. J Nucl Materials 320:280–291

Gibbons JF (1972) Ion implantation in semiconductors: Damage production and annealing. Proc IEEE 60:1062–1067

Glerup M, Nielsen OF, Poulsen FW (2001) The structural transformation from the pyrochlore structure, $A_2B_2O_7$ to the fluorite structure, AO_2, studied by Raman spectroscopy and defect chemistry modeling. J Solid State Chem 160:25–32

Gögen K, Wagner GA (2000) Alpha-recoil track dating of Quaternary volcanics. Chem Geol 166:127–137

Gong WL, Wang LM, Ewing RC, Zhang J (1996) Electron-irradiation- and ion-beam-induced amorphization of coesite. Phys Rev B 54:3800–3808

Gorshevskaya SA, Sidorenko GA, Smorchkov IE (1961) A new modification of fergusonite: β-fergusonite (abstract in Am Mineral 46:1516–1517). Geologiya Mestorozhdenii Redkikh Elementov 9:28–29

Janeczek J, Eby RK (1993) Annealing of radiation damage in allanite and gadolinite. Phys Chem Mineral 19:343–356

Karioris FG, Gowda KA, Cartz L, Labbe JC (1982) Damage cross-sections of heavy ions in crystal structures. J Nucl Materials 108/109:748–750

Keller C (1962) Über ternäre Oxide des Niobs and Tanatls vom Typ ABO_4. Z Anorg Allg Chem 318:89–106

Komkov AI (1959) Struktura prirodnogo fergusonita i ego polimorfioi modifikacii (in Russian). Crystallography 4:836–841

Lábár JL (2000) Proc. of EUREM 12, July 2000 Frank L, Ciampor F (eds) Vol. III, Brno, pp 1379–380

Laversenne L, Guyot Y, Goutaudier C, Cohen-Adad MTh, Boulon G (2001) Optimization of spectroscopic properties of Yb^{3+}-doped refractory sesquioxides: cubic Y_2O_3, Lu_2O_3 and monoclinic Gd_2O_3. Opt Mater 16:475–483

Lian J, Wang SX, Wang LM, Ewing RC (2001) Radiation damage and nanocrystal formation in uranium–niobium titanates. J Nucl Mater 297:89–96

Lian J, Wang L, Chen J, Sun K, Ewing RC, Matt Farmer J, Boatner LA (2003) The order–disorder transition in ion-irradiated pyrochlore. Acta Mater 51:1493–1502

Lumpkin GR, Ewing RC (1988) Alpha-decay damage in minerals of the pyrochlore group. Phys Chem Miner 16:2–20

Lumpkin GR, Ewing RC (1992) Geochemical alteration of pyrochlore group minerals: Microlite subgroup. Am Mineral 77:179–188

Lumpkin GR, Ewing RC (1995) Geochemical alteration of pyrochlore group minerals: Pyrochlore subgroup. Am Mineral 80:725–731

Lumpkin GR, Ewing RC (1996) Geochemical alteration of pyrochlore group minerals: Betafite subgroup. Am Mineral 81:1237–1248

Lumpkin RL, Smith KL, Blackford MG (2001) Heavy ion irradiation studies of columbite, brannnerite, and pyrochlore structure types. J Nucl Mater 289:177–187

Markiv VYa, Belyavina NM, Markiv MV, Titov YuA, Sych AM, Sokolov AN, Kapshuk AA, Slobodyanyk MS (2002) Peculiarities of polymorphic transformations in $YbTaO_4$ and crystal structure of its modifications. J Alloy Compound 346:263–268

Meldrum A, Wang LM, Ewing RC (1996) Ion-beam-induced amorphization of monazite. Nucl Instrum Meth B 116:220–224

Meldrum A, Boatner LA, Ewing RC (1997) Elecron-irradiation-induced nucleation and growth in amorphous $LaPO_4$, $ScPO_4$, and zircon. J Mater Res 12:1816–1827

Meldrum A, Boatner LA, Weber WJ, Ewing RC (1998) Radiation damage in zircon and monazite. Geochim Cosmochim Acta 62:2509–2520

Meldrum A, Boatner LA, Zinkle SJ, Wang SX, Wang LM, Ewing RC (1999) Effect of dose rate and temperature on the crystalline-to-metamict transformation in the ABO_4 orthosilicates. Can Mineral 37:207–221

Meldrum A, Boatner LA, Ewing RC (2000) A comparison of radiation effects in crystalline ABO_4-type phosphates and silicates. Mineral Mag 64:183–192

Motta AT (1997) Amorphization of intermetallic compounds under irradiation—a review. J Nucl Matter 244:227–250

Murakami T, Chakoumakos BC, Ewing RC, Lumpkin GR, Weber WJ (1991) Alpha-decay event damage in zircon. Am Mineral 76:1510–1532

Nasdala L, Irmer L, Wolf D (1995) The degree of metamictization in zircon: a Raman spectroscopic study. Eur J Mineral 7:471–478

Nasdala L, Lengauer CL, Hanchar JM, Kronz A, Wirth R, Blanc P, Kennedy AK, Seydoux-Guillaume AM (2002) Annealing radiation damage and the recovery of cathodoluminescence. Chem Geol 191:121–140

Nasdala L, Reiners PW, Garver JI, Kennedy AK, Stern RA, Balan E, Wirth R (2004a) Incomplete retention of radiation damage in zircon from Sri Lanka. Am Mineral 89:219–231

Nasdala L, Smith DC, Kaindl R, Ziemann MA (2004b) Raman spectroscopy: analytical perspectives in mineralogical research. In: Beran A, Libowitzky E (eds) Spectroscopic methods in mineralogy, European Mineralogical Union Notes in Mineralogy, vol. 6, Budapest, pp 281–343

Nasdala L, Wenzel M, Vavra G, Irmer F, Wenzel T, Kober B (2001) Metamictisation of natural zircon: accumulation versus thermal annealing of radioactivity-induced damage. Contrib Mineral Petr 141:125–144

Pouchou JL, Pichoir F (1991) Quantification analyses of homogeneous and stratified microvolumes applied model "PAP". In: Heinrich KFJ, Newbury DE (eds) Electron probe quantification. Plenum, New York pp 31–35

Powder Diffraction File (2004) Database Sets 1–54, International Centre for Diffraction Data (ICDD), Newtown Square

Rios S, Boffa-Ballaran T (2003) Microstructure of radiation-damaged zircon under pressure. J Appl Cryst 36:1006–1012

Rios S, Salje EKH, Zhang M, Ewing RC (2000) Amorphization in zircon: evidence for direct impact damage. J Phys Condens Matter 12:2401–2412

Seydoux-Guillaume AM, Wirth R, Nasdala L, Gottschalk M, Montel JM, Heinrich W (2002) An XRD, TEM and Raman study of experimentally annealed natural monazite. Phys Chem Miner 29:240–253

Shannon RD (1976) Revised effective ionic radii and systematic studies of interatomic distances in halides and chalcogenides. Acta Crystallogr A32:751–767

Sinclair W, Ringwood AE (1981) Alpha-recoil damage in natural zirconolite and perovskite. Geochem J 15:229–243

Tomašić N, Gajović A, Bermanec V, Rajić M (2004) Recrystallization of metamict Nb–Ta–Ti–REE complex oxides: a coupled X-ray-diffraction and Raman spectroscopy study of aeschynite-(Y) and polycrase-(Y). Can Mineral 42:1847–1857

Trachenko K, Pruneda M, Artacho E, Dove MT (2004) Radiation damage effects in the perovskite $CaTiO_3$ and resistance of materials to amorphization. Phys Rev B 70:134112

Wang LM, Eby RK, Janeczek J, Ewing RC (1991) In situ TEM study of ion-beam-induced amorphization of complex silicate structures. Nucl Instr Methods B 59/60:395–400

Wang SX, Wang LM, Ewing RC, Was GS, Lumpkin GR (1999) Ion irradiation-induced phase transformation of pyrochlore and zirconolite, Nucl Instr Meth B 148:704–709

Wang SX, Wang LM, Ewing RC (2000) Nano-scale glass formation in pyrochlore by ion irradiation. J Non-Cryst Solids 274:238–243

Weber WJ (1993) Alpha-decay-induced amorphization in complex silicate structures. J Am Ceram Soc 76:1729–1738

Weber WJ, Ewing RC, Catlow CRA, Diaz de la Rubia T, Hobbs LW, Kinoshita C, Matzke Hj, Motta AT, Nastasi M, Salje EKH, Vance ER, Zinkle SJ (1998) Radiation effects in crystalline ceramics for the immobilization of high-level nuclear waste and plutonium. J Mater Res 13:1434–1484

Weber WJ, Ewing RC, Wang LM (1994) The radiation-induced crystalline-to-amorphous transition in zircon. J Mater Res 9:688–698

Weitzel H, Schröcke H (1980) Kristallstrukturverfeinerungen von Euxenit, $Y(Nb_{0.5}Ti_{0.5})_2O_6$, und M-Fergusonit, $YNbO_4$. Z Kristallogr 152:69–82

Wolten GM (1967) The structure of the M'-phase of $YTaO_4$, a third fergusonite polymorph. Acta Crystallog 23:939–944

Wolten GM, Chase AB (1967) Synthetic fergusonites and a new polymorph of yttrium tantalite. Am Mineral 52:1536–1541

Yashima M, Lee JH, Kakihana M, Yoshimura M (1997) Raman spectral characterization of existing phases in the Y_2O_3–Nb_2O_5 system. J Phys Chem Solids 58:1593–1597

Yudintsev SV, Stefanovskii SV, Kir'yanova OI, Lian J, Ewing R (2001) Radiation resistance of fused titanium ceramic for actinide immobilization. Atom Energy 90:487–494

Zhang M, Salje EKH, Capitani GC, Leroux H, Clark AM, Schlüter, Ewing RC (2000a) Annealing of α-decay damage in zircon: a Raman spectroscopic study. J Phys Condens Matter 12:3131–3148

Zhang M, Salje EKH, Farnan I, Graeme-Barber A, Daniel P, Ewing RC, Clark AM, Leroux H (2000b) Metamictization of zircon: Raman spectroscopic study. J Phys Condens Matter 12:1915–1925